

Neutrino-Induced γ -Ray Emission from Supernovae

Yu Lu* and Yong-Zhong Qian†

School of Physics and Astronomy, University of Minnesota, Minneapolis, MN 55455

(Dated: December 4, 2018)

Abstract

During a core-collapse supernova, absorption of $\bar{\nu}_e$ emitted from the proto-neutron star by protons in the hydrogen envelope produces neutrons and positrons. Neutron capture on protons and positron annihilation then produce γ rays of 2.22 and 0.511 MeV, respectively. We calculate the fluxes of these γ rays expected from a supernova with an $11 M_{\odot}$ progenitor. The flux from neutron capture on protons exponentially decays on a timescale of 564 s, which is determined by neutron decay and capture on protons and ^3He nuclei. The peak flux is $2.38 \times 10^{-7} \text{ cm}^{-2} \text{ s}^{-1}$ for a supernova at a distance of 1 kpc. In contrast, the γ -ray flux from positron annihilation follows the time evolution of the $\bar{\nu}_e$ luminosity and lasts for ~ 10 s. The peak flux in this case is $6.8 \times 10^{-5} \text{ cm}^{-2} \text{ s}^{-1}$ for a supernova at a distance of 1 kpc. Detection of the above γ -ray fluxes is beyond the capability of current instruments, and perhaps even those planned for the near future. However, if such fluxes can be detected, they not only constitute a new kind of signals that occur during the gap of several hours between the neutrino signals and the optical display of a supernova, but may also provide a useful probe of the conditions in the surface layers of the supernova progenitor.

PACS numbers: 95.85.Pw, 97.60.Bw, 25.30.Pt

*Electronic address: ylu@physics.umn.edu

†Electronic address: qian@physics.umn.edu

I. INTRODUCTION

On exhaustion of nuclear fuels, the core of a massive star ($\gtrsim 8 M_\odot$ with M_\odot being the mass of the sun) undergoes gravitational collapse, thereby initiating the supernova process. Two classes of signals are expected from such an event: the neutrinos emitted by the proto-neutron star formed from the collapsed core and the photons radiated as the supernova shock emerges from the stellar surface. The neutrino signals start immediately after the shock is launched and last for ~ 10 s. However, it takes several hours for the shock to emerge, and consequently, the associated photon radiation, in particular the optical display, is delayed from the neutrino burst by this shock propagation time. In this paper we consider a third class of signals that occur before the shock emergence. These signals are γ rays induced by neutrino reactions in the stellar envelope.

We assume that the star undergoing core collapse still has its hydrogen envelope. As the neutrinos from the proto-neutron star stream through this envelope, the reaction



produces a neutron and a positron. Subsequently, the capture of the neutron through



produces a γ ray of 2.22 MeV, and the annihilation of the positron can produce two γ rays of 0.511 MeV each. The above mechanism of γ -ray emission from supernovae has been considered earlier by Refs. [1, 2]. However, these studies only estimated the expected γ -ray fluxes without giving an analysis of all the physical processes involved in the γ -ray production. For example, the thermalization of neutrons and positrons in the stellar envelope was not discussed, and neither was the detailed time structure of the γ -ray emission. We note that γ rays from neutron capture on protons and positron annihilation were also discussed in the context of solar flares (see e.g., Ref. [3]) and interstellar medium (see e.g., Ref. [4]), and there were extensive studies of the physical processes involved in the γ -ray emission from positron annihilation (see e.g., Ref. [5]).

We here present detailed analyses of the major physical processes that lead to γ -ray production following the reaction $\bar{\nu}_e + p \rightarrow n + e^+$ in the hydrogen envelope of a massive star. In particular, we show that the γ -ray emission due to neutron capture on protons

lasts for $\sim 10^3$ s while that due to positron annihilation follows the time evolution of the $\bar{\nu}_e$ luminosity and lasts for ~ 10 s. For concreteness, we adopt a specific model of neutrino emission and a specific stellar model for the conditions in the hydrogen envelope. Our analyses can be easily generalized to other neutrino emission and stellar models.

We assume that the gravitational binding energy E_B of the final neutron star is emitted equally in ν_e , $\bar{\nu}_e$, ν_μ , $\bar{\nu}_\mu$, ν_τ , and $\bar{\nu}_\tau$ and that the $\bar{\nu}_e$ luminosity $L_{\bar{\nu}_e}(t)$ decays exponentially on a timescale τ . Thus,

$$L_{\bar{\nu}_e}(t) = \frac{E_B}{6\tau} \exp(-t/\tau). \quad (3)$$

We take $E_B = 3 \times 10^{53}$ erg and $\tau = 3$ s. The normalized $\bar{\nu}_e$ energy spectrum is taken to be

$$f_{\bar{\nu}_e}(E_{\bar{\nu}_e}) = \frac{1}{T_{\bar{\nu}_e}^3 F_2(\eta_{\bar{\nu}_e})} \frac{E_{\bar{\nu}_e}^2}{\exp[(E_{\bar{\nu}_e}/T_{\bar{\nu}_e}) - \eta_{\bar{\nu}_e}] + 1}, \quad (4)$$

where $T_{\bar{\nu}_e} = 3.76$ MeV, $\eta_{\bar{\nu}_e} = 3$, and

$$F_n(\eta) \equiv \int_0^\infty \frac{x^n}{\exp(x - \eta) + 1} dx. \quad (5)$$

The corresponding average $\bar{\nu}_e$ energy is $\langle E_{\bar{\nu}_e} \rangle = T_{\bar{\nu}_e} F_3(\eta_{\bar{\nu}_e})/F_2(\eta_{\bar{\nu}_e}) = 15$ MeV. The cross section for the reaction $\bar{\nu}_e + p \rightarrow n + e^+$ (see Appendix A) averaged over the above spectrum is $\langle \sigma_{\bar{\nu}_e p} \rangle = 1.87 \times 10^{-41}$ cm².

For the conditions of the hydrogen envelope, we use the model of an $11 M_\odot$ star in Ref. [6]. The region of interest for γ -ray emission is limited by the interaction of γ rays with matter. For γ rays of ~ 1 MeV produced in the hydrogen envelope, the dominant interaction is Compton scattering on electrons. The relevant cross sections (see Appendix A) are $\sigma_{\gamma(np)e} = 1.38 \times 10^{-25}$ cm² and $\sigma_{\gamma(e^\pm)e} = 2.87 \times 10^{-25}$ cm² for γ rays of 2.22 and 0.511 MeV, respectively. The corresponding mean free path is

$$l_{\gamma e} = \frac{1}{n_e \sigma_{\gamma e}} = 1.66 \times 10^9 \left(\frac{10^{-8} \text{ g cm}^{-3}}{\rho Y_e} \right) \left(\frac{10^{-25} \text{ cm}^2}{\sigma_{\gamma e}} \right) \text{ cm}, \quad (6)$$

where $n_e = \rho Y_e N_A$ is the electron number density, ρ is the matter density, Y_e is the number of electrons per nucleon, and N_A is Avogadro's number. The surface zone of our adopted stellar model has $\rho = 1.59 \times 10^{-8}$ g cm⁻³ and $Y_e = 0.85$, for which $l_{\gamma(np)e} = 8.9 \times 10^8$ cm and $l_{\gamma(e^\pm)e} = 4.28 \times 10^8$ cm for γ rays of 2.22 and 0.511 MeV, respectively. The radius of this zone is $R = 2.36 \times 10^{13}$ cm. For considering the emission of 2.22 and 0.511 MeV γ rays (we do not treat the emission of scattered γ rays at other energies), it is sufficient to focus on the outermost region with a radial thickness d satisfying $l_{\gamma e} \ll d \ll R$. The stellar conditions

stay constant in this region. In addition, the rate for production of neutrons and positrons per nucleon by the reaction $\bar{\nu}_e + p \rightarrow n + e^+$ is the same throughout this region and is

$$\lambda_{\bar{\nu}_ep}(t) = Y_p \left(\frac{\langle \sigma_{\bar{\nu}_ep} \rangle}{4\pi R^2} \right) \frac{L_{\bar{\nu}_e}(t)}{\langle E_{\bar{\nu}_e} \rangle} = \lambda_{\bar{\nu}_ep}(0) \exp(-t/\tau), \quad (7)$$

where $Y_p = 0.7$ is the number of protons per nucleon in the region, and $\lambda_{\bar{\nu}_ep}(0) = 1.30 \times 10^{-12} \text{ s}^{-1}$ for the adopted parameters.

We study the emission of 2.22 MeV γ rays from neutron capture on protons in Sec. II and that of 0.511 MeV γ rays from positron annihilation in Sec. III. We discuss our results and give conclusions in Sec. IV.

II. γ -RAY EMISSION FROM NEUTRON CAPTURE ON PROTONS

Before discussing the physical processes leading to γ -ray emission from neutron capture on protons, we give a simple estimate of the time evolution of the corresponding flux. This evolution is closely related to that of the neutron number per nucleon $Y_n(t)$ in the stellar surface region from which γ rays can escape efficiently. The increase in $Y_n(t)$ is due to $\bar{\nu}_e$ absorption by protons with the rate $\lambda_{\bar{\nu}_ep}(t)$ given in Eq. (7). The decrease in $Y_n(t)$ is caused by neutron decay and capture onto protons and ^3He . The neutron lifetime is $\tau_n = 887 \text{ s}$. For capture of low-energy neutrons, the cross section is inversely proportional to the neutron velocity v_n . Consequently, the product of the cross section and v_n is independent of the neutron velocity distribution. We use $\langle v_n \sigma_{np} \rangle = 7.32 \times 10^{-20} \text{ cm}^3 \text{ s}^{-1}$ for capture onto protons and $\langle v_n \sigma_{n3} \rangle = 1.17 \times 10^{-15} \text{ cm}^3 \text{ s}^{-1}$ for capture onto ^3He . The corresponding capture timescales are $\tau_{np} = (\rho Y_p N_A \langle v_n \sigma_{np} \rangle)^{-1} = 2.04 \times 10^3 \text{ s}$ and $\tau_{n3} = (\rho Y_3 N_A \langle v_n \sigma_{n3} \rangle)^{-1} = 6.38 \times 10^3 \text{ s}$, where we have taken the number of ^3He per nucleon to be $Y_3 = 1.4 \times 10^{-5}$, the same as estimated for the solar photosphere [3]. Note that the dominant channel of neutron capture onto ^3He is $n + ^3\text{He} \rightarrow p + ^3\text{H}$, which does not produce any γ ray. However, the enormous cross section of this channel enables it to play a significant role in determining the evolution of $Y_n(t)$ in spite of the small abundance of ^3He .

A simple estimate of $Y_n(t)$ can be obtained from

$$\frac{dY_n}{dt} = \lambda_{\bar{\nu}_ep}(t) - \frac{Y_n(t)}{\tau_{\text{eff}}}, \quad (8)$$

where $\tau_{\text{eff}}^{-1} = \tau_n^{-1} + \tau_{np}^{-1} + \tau_{n3}^{-1}$ and $\tau_{\text{eff}} = 564$ s. The solution to the above equation is

$$Y_n(t) = \lambda_{\bar{\nu}_e p}(0)\tau \left(\frac{\tau_{\text{eff}}}{\tau_{\text{eff}} - \tau} \right) [\exp(-t/\tau_{\text{eff}}) - \exp(-t/\tau)]. \quad (9)$$

As $\tau_{\text{eff}} \gg \tau$, $Y_n(t)$ rises to its peak value

$$Y_n^{\text{pk}} \approx \lambda_{\bar{\nu}_e p}(0)\tau = 3.90 \times 10^{-12} \quad (10)$$

on a timescale of ~ 10 s and then exponentially decays on the timescale τ_{eff} .

Due to Compton scattering, only those γ -rays of 2.22 MeV produced in the outermost stellar layer with a thickness of $\sim l_{\gamma(np)e} = 8.9 \times 10^8$ cm will escape efficiently. The corresponding flux at a radius $r > R$ can be estimated as

$$\Phi_{\gamma(np)}(r, t_r) \sim \frac{\rho Y_n(t) N_A R^2 l_{\gamma(np)e}}{\tau_{np} r^2} \sim 9.53 \times 10^{-7} \left(\frac{1 \text{ kpc}}{r} \right)^2 \exp(-t/\tau_{\text{eff}}) \text{ cm}^{-2} \text{ s}^{-1}, \quad (11)$$

where t_r is the time at which the γ rays emitted at time t arrive at radius r and we have used $Y_n(t) \sim Y_n^{\text{pk}} \exp(-t/\tau_{\text{eff}})$ in the second approximation. To show the dependence on the model of neutrino emission and stellar conditions, we rewrite the above equation as

$$\Phi_{\gamma(np)}(r, t_r) \sim \frac{E_B}{24\pi r^2 \langle E_{\bar{\nu}_e} \rangle \tau_{np}} \left(\frac{Y_p \langle \sigma_{\bar{\nu}_e p} \rangle}{Y_e \sigma_{\gamma(np)e}} \right) \exp(-t/\tau_{\text{eff}}). \quad (12)$$

It can be seen that the exact form of $L_{\bar{\nu}_e}(t)$ is unimportant so long as the timescale of neutrino emission is $\ll \tau_{\text{eff}}$. In addition, the density of the stellar surface region controls the peak magnitude and the decay timescale of the flux via τ_{np} and τ_{eff} , respectively. Integrating the flux over time, we estimate the total fluence of 2.22 MeV γ rays at radius r as

$$\mathcal{F}_{\gamma(np)} \sim \frac{E_B}{24\pi r^2 \langle E_{\bar{\nu}_e} \rangle} \left(\frac{Y_p \langle \sigma_{\bar{\nu}_e p} \rangle}{Y_e \sigma_{\gamma(np)e}} \right) \left(\frac{\tau_{\text{eff}}}{\tau_{np}} \right) \sim 5.37 \times 10^{-4} \left(\frac{1 \text{ kpc}}{r} \right)^2 \text{ cm}^{-2}. \quad (13)$$

Note that $\mathcal{F}_{\gamma(np)}$ in general still depends on the density of the stellar surface region due to the competition between neutron decay and capture. This dependence ceases only when neutron decay can be ignored (i.e., $\tau_n \gg \tau_{np}$).

A. Thermalization and Diffusion of Neutrons

As discussed above, the timescales for neutron capture onto protons and ${}^3\text{He}$ are $\tau_{np} = 2.04 \times 10^3$ s and $\tau_{n3} = 6.38 \times 10^3$ s for the adopted density and composition of the stellar surface region. We now show that these timescales and the neutron lifetime are so long

that neutrons are thermalized due to scattering by protons before being captured or decay. Following the absorption of $\bar{\nu}_e$ by protons, positrons are emitted approximately isotropically with energies of $\approx E_{\bar{\nu}_e}$. Using the $\bar{\nu}_e$ energy spectrum in Eq. (4) and the cross section in Eq. (A1), we obtain the average recoil energy of the neutrons produced along with the positrons as $\langle E_n^{\text{rec}} \rangle \sim [F_6(\eta_{\bar{\nu}_e})/F_4(\eta_{\bar{\nu}_e})]T_{\bar{\nu}_e}^2/M_n \sim 543$ keV, where M_n is the neutron rest mass. The region of interest has a temperature $T = 1.53 \times 10^4$ K corresponding to a thermal energy $E_{\text{th}} = (3/2)kT = 1.98$ eV $\ll \langle E_n^{\text{rec}} \rangle$ with k being Boltzmann's constant. Consequently, neutrons lose energy through scattering by thermal protons until neutrons are thermalized (scattering by other particles can be ignored). The average decrease in the natural logarithm of neutron energy per scattering is unity [7]: $\langle \ln(E_{n,j+1}/E_{n,j}) \rangle = -1$, where $E_{n,j}$ is the neutron energy after j scatterings. So we approximately have

$$E_{n,j} \sim \langle E_n^{\text{rec}} \rangle \exp(-j). \quad (14)$$

The mean free path between scattering is

$$l_{\text{sc}} = \frac{1}{n_p \sigma_{\text{sc}}} = 1.66 \times 10^7 \left(\frac{10^{-8} \text{ g cm}^{-3}}{\rho Y_p} \right) \left(\frac{10 \text{ b}}{\sigma_{\text{sc}}} \right) \text{ cm}, \quad (15)$$

where $n_p = \rho Y_p N_A$ is the proton number density and σ_{sc} is the scattering cross section. For the relevant neutron energies, $\sigma_{\text{sc}} \sim 10$ b [8] corresponds to $l_{\text{sc}} \sim 1.49 \times 10^7$ cm for the adopted stellar conditions. The timescale for thermalization can then be estimated as

$$\tau_{\text{therm}} \sim \sum_{j=0}^{j_{\text{max}}-1} \frac{l_{\text{sc}}}{\sqrt{2E_{n,j}/M_n}} \sim 15 \text{ s} \ll \tau_n, \tau_{np}, \tau_{n3}, \quad (16)$$

where $j_{\text{max}} \sim \ln(\langle E_n^{\text{rec}} \rangle / E_{\text{th}}) \sim 13$.

Once thermalized, neutrons diffuse until they decay or are captured or escape from the stellar surface. The mean speed of thermal neutrons is $\bar{v}_n = \sqrt{8kT/(\pi M_n)} = 1.80 \times 10^6$ cm s⁻¹. If they escape from the star under consideration ($11 M_\odot$ with a radius $R = 2.36 \times 10^{13}$ cm), they will not fall back onto the star as they will decay while they are still moving away from the star. Therefore, those neutrons that can escape will not contribute to the production of γ rays. In order to escape, neutrons must diffuse to the stellar surface on timescales shorter than τ_{eff} . The thickness δ of the layer from which neutrons can diffuse to escape can be estimated from $\delta^2 \sim (\bar{v}_n \tau_{\text{eff}} / l_{\text{sc,th}}) l_{\text{sc,th}}^2$, which gives $\delta \sim \sqrt{\bar{v}_n \tau_{\text{eff}} l_{\text{sc,th}}} = 8.6 \times 10^7$ cm with $l_{\text{sc,th}} = 7.28 \times 10^6$ cm corresponding to $\sigma_{\text{sc,th}} = 20.5$ b for thermal neutrons. As $\delta \sim 0.1 l_{\gamma(np)e}$, the reduction of potential γ -ray production due to the escape

TABLE I: Rate, mean free paths, and timescales for the important processes involved in the γ -ray emission from neutron capture on protons. The adopted conditions in the stellar surface region are characterized by $R = 2.36 \times 10^{13}$ cm, $\rho = 1.59 \times 10^{-8}$ g cm $^{-3}$, $Y_e = 0.85$, $Y_p = 0.7$, and $Y_3 = 1.4 \times 10^{-5}$.

$\lambda_{\bar{\nu}_e p}(0)$	$l_{\gamma(np)e}$	$l_{\text{sc,th}}$	τ_{np}	τ_{n3}	τ_{eff}
1.30×10^{-12} s $^{-1}$	8.9×10^8 cm	7.28×10^6 cm	2.04×10^3 s	6.38×10^3 s	564 s

of neutrons is insignificant. For the outmost layer of thickness $l_{\gamma(np)e}$ from which γ rays can escape efficiently, essentially all the neutrons in this layer decay or are captured by protons or ^3He during diffusion. Indeed, the timescale for neutrons to diffuse out of this layer is

$$\tau_{\text{diff}} = \frac{l_{\gamma(np)e}^2}{l_{\text{sc,th}} \bar{v}_n} = 6.04 \times 10^4 \text{ s} \gg \tau_{\text{eff}}. \quad (17)$$

For the adopted stellar conditions, $\tau_n = \tau_{np}/2.3$ and $\tau_{n3} = 3.1\tau_{np}$. So a fraction $\tau_{\text{eff}}/\tau_{np} = [1 + (\tau_{np}/\tau_n) + (\tau_{np}/\tau_{n3})]^{-1} = 27.6\%$ of the neutrons are captured by protons to produce 2.22 MeV γ rays. The reduction of potential γ -ray production is mainly due to neutron decay and to a smaller extent due to neutron capture by ^3He . The rates and mean free paths for the important processes involved in the γ -ray emission from neutron capture on protons in the star under consideration are summarized in Table I.

B. Evolution of Neutron Density and Emergent γ -Ray Flux

Based on the preceding discussion, we consider the following quantitative model for calculating the flux of 2.22 MeV γ rays from the star under consideration. We focus on the outermost layer of thickness $d = 10^{10}$ cm $\gg l_{\gamma(np)e}$ to find the emergent flux $\Phi_{\gamma(np)}(R, t)$ at the stellar surface. As $d \ll R$, we can treat the layer of interest as a slab perpendicular to the x -axis with the stellar surface at $x = d$ (see Fig. 1). Knowing the neutron number per nucleon $Y_n(x, t)$ in this layer, we can calculate the local flux of 2.22 MeV γ rays in the positive x -direction as

$$\frac{Y_n(x, t) \rho N_A}{4\pi \tau_{np}} \int_0^{\pi/2} \cos \theta \sin \theta d\theta \int_0^{2\pi} d\phi = \frac{Y_n(x, t) \rho N_A}{4\tau_{np}}, \quad (18)$$

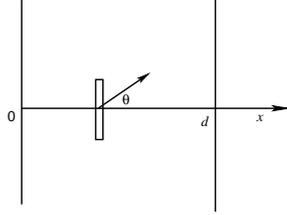


FIG. 1: Sketch of the stellar surface region of interest to γ -ray emission. As $l_{\gamma e} \ll d \ll R$, this region can be treated as a slab of thickness d perpendicular to the x -axis with the surface at $x = d$. The calculation of the local γ -ray flux in the positive x -direction involves integration over the forward solid angle defined by $0 \leq \theta \leq \pi/2$.

where θ and ϕ are respectively, the polar and azimuthal angles with respect to the x -axis. Consequently, the emergent flux at the stellar surface is

$$\Phi_{\gamma(np)}(R, t) = \frac{\rho N_A}{4\tau_{np}} \int_0^d Y_n(x, t) \exp\left(-\frac{d-x}{l_{\gamma(np)e}}\right) dx, \quad (19)$$

which is related to the flux at $r > R$ as $\Phi_{\gamma(np)}(r, t_r) = (R/r)^2 \Phi_{\gamma(np)}(R, t)$.

The evolution of $Y_n(x, t)$ is governed by diffusion:

$$\frac{\partial Y_n}{\partial t} = D \frac{\partial^2 Y_n}{\partial x^2} - \frac{Y_n(x, t)}{\tau_{\text{eff}}}, \quad (20)$$

where $D = l_{\text{sc,th}} \bar{v}_n / 3$ is the diffusion coefficient of thermal neutrons. As τ_{eff} is much longer than the timescales for neutrino emission and thermalization of neutrons, we assume $Y_n(x, 0) = Y_n^{\text{pk}}$ [see Eq. (10)]. Further, on the timescale relevant for γ -ray production, diffusion has little effect on the spatial distribution of neutrons at $x = 0$ [see Eq. (17)]. So we take $(\partial Y_n / \partial x)_{x=0} = 0$ as the inner boundary condition. For the outer boundary at $x = d$, we assume that the drift neutron flux given by diffusion is the same as the escaping neutron flux: $-D(\partial Y_n / \partial x)_{x=d} = \bar{v}_n Y_n(d, t) / 4$, which is equivalent to $l_{\text{sc,th}}(\partial Y_n / \partial x)_{x=d} = -(3/4)Y_n(d, t)$. With the initial and boundary conditions discussed above, the solution to Eq. (20) is

$$Y_n(x, t) = 2Y_n^{\text{pk}} \sum_{j=0}^{\infty} \frac{\sin(\kappa_j d) \cos(\kappa_j x)}{\kappa_j d + \sin(\kappa_j d) \cos(\kappa_j d)} \exp[-(\kappa_j^2 D + \tau_{\text{eff}}^{-1})t], \quad (21)$$

where κ_j satisfies $\kappa_j l_{\text{sc,th}} \tan(\kappa_j d) = 3/4$ as required by the outer boundary condition. The evolution of $Y_n(x, t)$ given by Eq. (21) is shown in Fig. 2a.

Substituting the above expression of $Y_n(x, t)$ in Eq. (19), we obtain

$$\Phi_{\gamma(np)}(R, t) = \frac{Y_n^{\text{pk}} \rho N_A l_{\gamma(np)e}}{2\tau_{np}} \sum_{j=0}^{\infty} A_j \exp[-(\kappa_j^2 D + \tau_{\text{eff}}^{-1})t] \quad (22)$$

where

$$A_j = \frac{\sin(\kappa_j d) [\cos(\kappa_j d) + (\kappa_j l_{\gamma(np)e}) \sin(\kappa_j d) - \exp(-d/l_{\gamma(np)e})]}{[\kappa_j d + \sin(\kappa_j d) \cos(\kappa_j d)] [1 + (\kappa_j l_{\gamma(np)e})^2]}. \quad (23)$$

As $l_{\text{sc,th}} \ll l_{\gamma(np)e} \ll d$, it can be shown that

$$A_j \approx \frac{l_{\gamma(np)e}/d}{[1 + (4\kappa_j l_{\text{sc,th}}/3)^2] [1 + (\kappa_j l_{\gamma(np)e})^2]}. \quad (24)$$

The outer boundary condition gives $j\pi/d < \kappa_j < [(j + (1/2))\pi/d]$. For $j \ll 3d/(4\pi l_{\text{sc,th}}) = 328$, $\kappa_j \approx [j + (1/2)]\pi/d$. This approximation can be used for all j as there is little difference between j and $j + (1/2)$ for sufficiently large j . Noting that $4\kappa_j l_{\text{sc,th}}/3 \approx [j + (1/2)]/328$, $\kappa_j l_{\gamma(np)e} \approx [j + (1/2)]/3.58$, and $\kappa_j^2 D\tau_{\text{eff}} \approx \{[j + (1/2)]/64.1\}^2$, we have

$$\begin{aligned} \Phi_{\gamma(np)}(r, t_r) &= \left(\frac{R}{r}\right)^2 \Phi_{\gamma(np)}(R, t) \\ &\approx \frac{Y_n^{\text{pk}} \rho N_A R^2 l_{\gamma(np)e}}{2\tau_{np} r^2} \exp(-t/\tau_{\text{eff}}) \sum_{j=0}^{\infty} \frac{l_{\gamma(np)e}/d}{1 + \{[j + (1/2)]\pi l_{\gamma(np)e}/d\}^2} \end{aligned} \quad (25)$$

$$\approx 2.38 \times 10^{-7} \left(\frac{1 \text{ kpc}}{r}\right)^2 \exp(-t/\tau_{\text{eff}}) \text{ cm}^{-2} \text{ s}^{-1}. \quad (26)$$

The result in Eq. (26) is obtained by approximating the sum in Eq. (25) by the integral $\int_0^\infty (1 + y^2)^{-1} dy/\pi = 1/2$. This result is smaller than the estimate in Eq. (11) by a factor of 4, which comes from the integration over the solid angle to obtain the local flux at a point in the region of γ -ray production [see Eq. (18)]. We numerically evaluate the flux of 2.22 MeV γ rays at $r = 1$ kpc as a function of time t from Eqs. (22) and (23) and show the result in Fig. 2b along with the approximation in Eq. (26). The numerical result is essentially the same as the approximation.

III. γ -RAY EMISSION FROM POSITRON ANNIHILATION

The processes leading to the emission of 0.511 MeV γ rays from annihilation of positrons subsequent to their production by $\bar{\nu}_e$ absorption on protons are much more complicated than those resulting in the emission of 2.22 MeV γ rays from neutron capture on protons. This is because a positron can lose energy through many processes such as electronic excitations of ionized and atomic matter, bremsstrahlung, Compton scattering, and synchrotron radiation in the presence of a magnetic field. In addition, a positron can directly annihilate with or

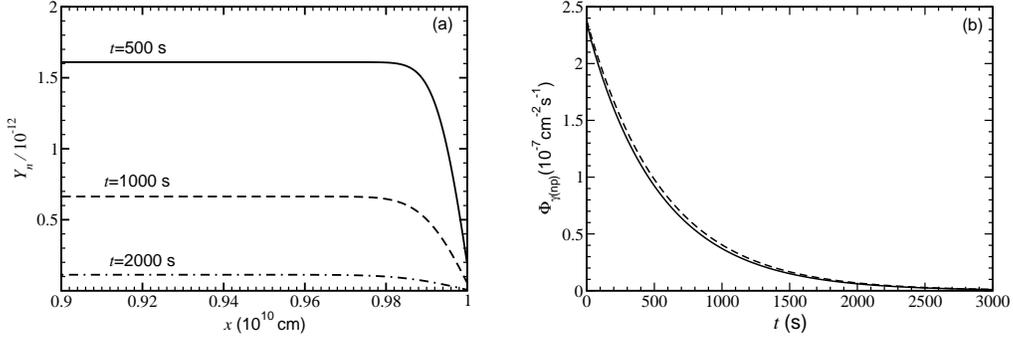


FIG. 2: (a) Neutron number per nucleon $Y_n(x, t)$ as functions of x in the stellar surface region for $t = 500, 1000,$ and 2000 s. Note that the decline of $Y_n(x, t)$ with x due to diffusion only occurs in a narrow region near the surface. (b) Time evolution for the expected flux of 2.22 MeV γ rays from neutron capture on protons in a supernova at a distance of 1 kpc as calculated by solving the diffusion equation (solid curve) and estimated by neglecting diffusion (dashed curve).

form a positronium (Ps) with a free or bound electron:



In the case of Ps formation (with free and bound electrons through radiative combination and charge exchange, respectively), the singlet Ps (^1Ps with total spin 0) decays by emitting two photons of 0.511 MeV each while the triplet Ps (^3Ps with total spin 1) decays by emitting three photons with a continuous energy spectrum. Here we focus on the production of 0.511 MeV γ rays only. We will loosely refer to both direct annihilation of positrons and Ps decay as “annihilation” of positrons.

The energy loss and the annihilation processes of the positrons depend on the ionization state of the medium. We consider that the stellar surface region is in local thermodynamic equilibrium at $T = 1.53 \times 10^4$ K and $\rho = 1.59 \times 10^{-8} \text{ g cm}^{-3}$. We assume that the forward

and reverse processes of the following chemical reactions are in equilibrium:



As we will see shortly, nearly all of the He atoms remain neutral and therefore, we can ignore the presence of He^{++} . To avoid confusion, we denote the numbers of free e^- , H^+ (free protons), He^+ , and neutral H and He atoms per nucleon as Y_{e^-} , Y_{H^+} , Y_{He^+} , Y_{H} , and Y_{He} , respectively. These quantities satisfy

$$Y_{\text{H}^+} + Y_{\text{H}} = Y_p, \quad (35)$$

$$Y_{\text{He}^+} + Y_{\text{He}} = Y_\alpha, \quad (36)$$

$$Y_{\text{H}^+} + Y_{\text{He}^+} = Y_{e^-}, \quad (37)$$

where $Y_p = 0.7$ and $Y_\alpha = 0.075$ are the numbers of protons and ${}^4\text{He}$ nuclei per nucleon, respectively ($Y_p + 4Y_\alpha = 1$ for consistency with a medium where the dominant nuclei are protons and α particles).

Based on the chemical equilibrium for the reactions in Eqs. (33) and (34), we obtain

$$\frac{Y_{\text{H}}}{Y_{\text{H}^+}} = \rho Y_{e^-} N_A \left(\frac{g_{\text{H}}}{4}\right) \left(\frac{2\pi\hbar^2}{m_e kT}\right)^{3/2} \exp\left(\frac{I_{\text{H}}}{kT}\right) = 7.47 \times 10^{-2} Y_{e^-}, \quad (38)$$

$$\frac{Y_{\text{He}^+}}{Y_{\text{He}}} = \frac{1}{\rho Y_{e^-} N_A} \left(\frac{2g_{\text{He}^+}}{g_{\text{He}}}\right) \left(\frac{m_e kT}{2\pi\hbar^2}\right)^{3/2} \exp\left(-\frac{I_{\text{He}}}{kT}\right) = \frac{1.52 \times 10^{-2}}{Y_{e^-}}, \quad (39)$$

where m_e is the electron rest mass, $g_{\text{H}} \approx 4.8$, $g_{\text{He}^+} \approx 2$, and $g_{\text{He}} \approx 1$ are the partition functions of the corresponding species, and $I_{\text{H}} = 13.6$ eV and $I_{\text{He}} = 24.6$ eV are the first ionization potentials for the ground states of the H and He atoms, respectively. There is some subtlety in calculating the partition functions as discussed in Appendix B. However, this does not affect the general results: nearly all of the H atoms are ionized and nearly all of the He atoms remain neutral. Solving Eqs. (35)–(39), we obtain $Y_{e^-} \approx 0.67$, $Y_{\text{H}^+} \approx 0.667$, $Y_{\text{H}} \approx 0.033$, $Y_{\text{He}} \approx 7.33 \times 10^{-2}$, and $Y_{\text{He}^+} \approx 1.7 \times 10^{-3}$.

The positrons produced by $\bar{\nu}_e$ absorption on protons have an average energy $\langle E_{e^+} \rangle \sim [F_5(\eta_{\bar{\nu}_e})/F_4(\eta_{\bar{\nu}_e})]T_{\bar{\nu}_e} \sim 21.2$ MeV. As they pass through the essentially ionized plasma of the stellar surface region, they can lose energy through many processes, directly annihilate, and form Ps. The ${}^1\text{Ps}$ formed decays into two photons with an extremely short lifetime of $\tau_{2\gamma} = 1.25 \times 10^{-10}$ s while the ${}^3\text{Ps}$ decays into three photons with a much longer lifetime of

$\tau_{3\gamma} = 1.42 \times 10^{-7}$ s. Consequently, once formed, ^1Ps immediately decays while ^3Ps can be broken up or converted into ^1Ps by the following reactions before it decays:

$$e^- + ^3\text{Ps} \rightarrow e^- + e^+ + e^-, \quad (40)$$

$$\text{H} + ^3\text{Ps} \rightarrow \text{H} + e^+ + e^-, \quad (41)$$

$$\text{H}^+ + \text{Ps} \rightarrow \text{H} + e^+, \quad (42)$$

$$\text{He}^+ + \text{Ps} \rightarrow \text{He} + e^+, \quad (43)$$

$$e^- + ^3\text{Ps} \rightarrow e^- + ^1\text{Ps}, \quad (44)$$

$$\text{H} + ^3\text{Ps} \rightarrow \text{H} + ^1\text{Ps}. \quad (45)$$

Note that the breakup reactions in Eqs. (42) and (43) are the reverse processes of the Ps formation reactions in Eqs. (31) and (32). Although all the processes in Eqs. (27)–(32) and (40)–(45) are involved (to varying degrees) in the γ -ray emission from positron annihilation (see Fig. 3a), for the adopted stellar conditions, the net result is rather simple: (1) Before thermalization, $\approx 12\%$ of the positrons directly annihilate and $\approx 4\%$ form Ps. Based on the available spin states, 1/4 of the Ps formed are ^1Ps , which immediately decay into two 0.511 MeV γ rays with line widths of ~ 6 keV, and 3/4 of the Ps formed are ^3Ps , which are immediately broken up (see Fig. 3b). The positrons released by breakup of ^3Ps are quickly thermalized. (2) So effectively $\approx 87\%$ of the initial positrons are thermalized. Essentially all of the thermal positrons form Ps. The ^3Ps formed are immediately broken up or converted into ^1Ps (see Fig. 3c). The positrons released by breakup of ^3Ps are again quickly thermalized. All the ^1Ps formed after thermalization immediately decay into two 0.511 MeV γ rays with line widths of ~ 2 keV.

A. Thermalization of Positrons

As mentioned above, positrons can lose energy through many processes. For the adopted stellar conditions, the dominant energy loss is due to excitation of the free electrons in the plasma. The thermalization of positrons spans the highly relativistic and nonrelativistic regimes. We use the general results on positron interaction with plasma electrons given in Ref. [9]. In the relativistic regime, the energy loss per unit length of propagation is

$$-\left(\frac{dE_{e^+}}{dx}\right)_{\text{ex,pl}} = 4\pi\rho Y_{e^-} N_A \left(\frac{e^4}{m_e v^2}\right) B_{\text{rel}} = 4.88 \times 10^{-9} \left(\frac{c}{v}\right)^2 Y_{e^-} B_{\text{rel}} \text{ MeV cm}^{-1}, \quad (46)$$

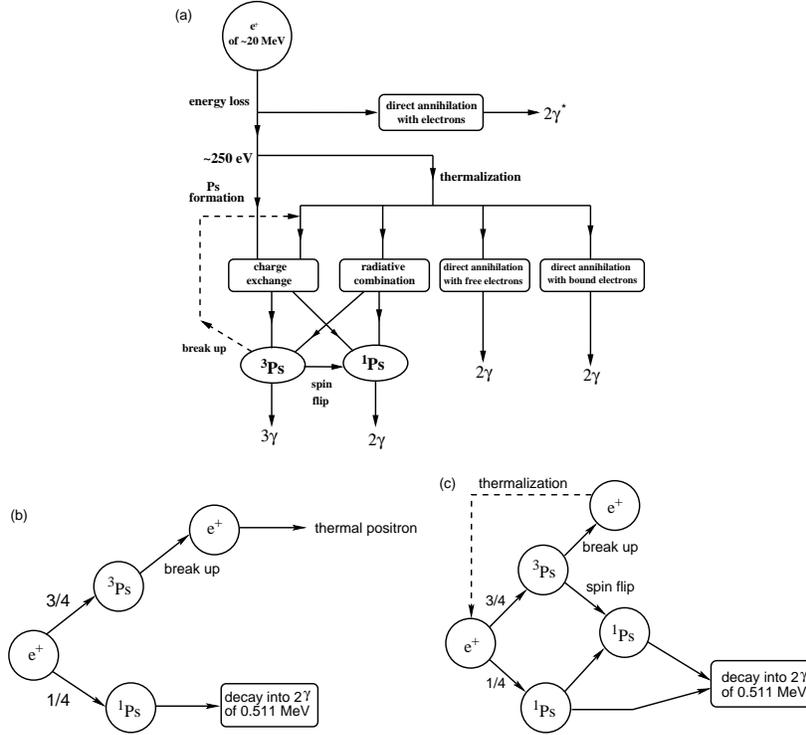


FIG. 3: (a) Summary of the processes involved in the γ -ray emission from annihilation of positrons with an initial energy of ~ 20 MeV. Direct annihilation with electrons before thermalization produces γ rays (indicated by γ^*) with energies shifted far from 0.511 MeV. Positronium (Ps) formation with free and bound electrons is referred to as radiative combination and charge exchange, respectively. (b) Summary of the consequences of Ps formation that occurs after the positron *kinetic* energy drops below ~ 250 eV but before thermalization. (c) Summary of the consequences of Ps formation after thermalization.

where

$$B_{\text{rel}} = \ln \left[\frac{\sqrt{2\delta(\gamma-1)} m_e v c}{\hbar \omega_p} \right] + b(\gamma, \delta). \quad (47)$$

In the above equations, v is the positron velocity, c is the speed of light, $\gamma \equiv 1/\sqrt{1-(v/c)^2}$, δ is the maximum fraction of the positron energy lost in a single interaction and is taken to

be $1/2$, $\omega_p = \sqrt{4\pi\rho Y_{e^-} N_A e^2 / m_e}$ is the plasma frequency, and

$$\begin{aligned}
b(\gamma, \delta) \equiv & -\left(\frac{\gamma^2 - 1}{2\gamma^2}\right) \delta + \frac{1}{8} \left(\frac{\gamma - 1}{\gamma}\right)^2 \delta^2 \\
& - \frac{1}{2} \left(\frac{\gamma - 1}{\gamma + 1}\right) \left[\left(\frac{\gamma + 2}{\gamma}\right) \delta - \left(\frac{\gamma^2 - 1}{\gamma^2}\right) \delta^2 + \frac{1}{3} \left(\frac{\gamma - 1}{\gamma}\right)^2 \delta^3 \right] \\
& + \frac{1}{2} \left(\frac{\gamma - 1}{\gamma + 1}\right)^2 \left[\left(\frac{1}{2} + \frac{1}{\gamma} + \frac{3}{2\gamma^2}\right) \frac{\delta^2}{2} - \left(\frac{\gamma - 1}{\gamma}\right)^2 \left(\frac{\delta^3}{3} - \frac{\delta^4}{4}\right) \right]. \quad (48)
\end{aligned}$$

The energy loss rate in the nonrelativistic regime is obtained by replacing B_{rel} in Eq. (46) with

$$B_{\text{nr}} = \ln \left[\frac{\sqrt{\delta} m_e v^2}{\hbar \omega_p} \right] - \varepsilon - \Re \psi(i\alpha c/v), \quad (49)$$

where $\varepsilon \approx 0.577$ is Euler's constant, $\alpha = e^2/(\hbar c)$ is the fine-structure constant, and $\Re \psi(z)$ is the real part of the digamma function $\psi(z) \equiv (d\Gamma/dz)/\Gamma(z)$ with $\Gamma(z)$ being the Gamma function.

The positrons produced by $\bar{\nu}_e$ absorption on protons have an average energy $\langle E_{e^+} \rangle \sim 21.2$ MeV corresponding to $\langle \gamma \rangle \sim 41.5$. Once thermalized, they have an average *kinetic* energy $E_{\text{th}} = (3/2)kT = 1.98$ eV corresponding to $\gamma_{\text{th}} - 1 = 3.87 \times 10^{-6}$. Using the energy loss rate discussed above, we can estimate the total distance $(\Delta x)_{\text{th}}$ and time $(\Delta t)_{\text{th}}$ covered by a typical positron during thermalization. We proceed by noting that both $-(dE_{e^+}/dx)_{\text{ex,pl}}$ and $-(dE_{e^+}/dt)_{\text{ex,pl}} = -v(dE_{e^+}/dx)_{\text{ex,pl}}$ increase as the positron energy decreases. Consequently, the bulk of $(\Delta x)_{\text{th}}$ and $(\Delta t)_{\text{th}}$ is covered before positrons become nonrelativistic, and we obtain

$$(\Delta x)_{\text{th}} \sim \int_{\langle E_{e^+} \rangle}^{m_e c^2} \frac{dE_{e^+}}{(dE_{e^+}/dx)_{\text{ex,pl}}} \sim \frac{\langle E_{e^+} \rangle}{4\pi\rho Y_{e^-} N_A [e^4/(m_e c^2)] B_{\text{rel}}} \sim 3 \times 10^8 \text{ cm}, \quad (50)$$

where we have taken advantage of the slowly-varying function B_{rel} in evaluating the integral and used $B_{\text{rel}} \sim 20$ for the adopted stellar conditions. The distance $(\Delta x)_{\text{th}}$ estimated above corresponds to a thermalization timescale $(\Delta t)_{\text{th}} \sim (\Delta x)_{\text{th}}/c \sim 10^{-2}$ s.

The energy loss rate discussed above is shown as a function of $\gamma - 1$ in Fig. 4. For comparison, the rates due to the other processes discussed in Appendix C are also shown. It can be seen that the energy loss due to excitation of the free electrons in the plasma dominates over the entire energy range between production and thermalization of positrons. We have numerically evaluated $(\Delta x)_{\text{th}}$ and $(\Delta t)_{\text{th}}$ first using the actual energy loss rate due

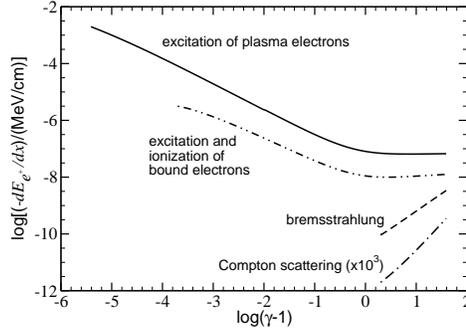


FIG. 4: Rates of positron energy loss $-dE_{e+}/dx$ as functions of $\gamma - 1$ for excitation of free electrons in the plasma (solid curve), excitation and ionization of bound electrons in atoms (dash-dot-dotted curve), bremsstrahlung (dashed curve), and Compton scattering on thermal photons (dashed-dotted curve). The rate for the first process is shown down to a positron *kinetic* energy of 2 eV (the thermal energy for the stellar conditions adopted here), that for the second process is shown down to a positron *kinetic* energy of 100 eV (the average excitation energy being 15 and 41.5 eV for H and He atoms, respectively), and those for the last two processes are shown only for relativistic positrons with $\gamma \geq 3$. Note that the actual rate multiplied by a factor of 10^3 is shown for Compton scattering.

to excitation of the free electrons in the plasma only and then including the actual rates of the other processes discussed in Appendix C. The inclusion of the other processes has rather small effect and reduces $(\Delta x)_{\text{th}}$ from 2.98×10^8 to 2.49×10^8 cm and $(\Delta t)_{\text{th}}$ from 10^{-2} to 8.4×10^{-3} s.

B. Direct Annihilation of Positrons before Thermalization

In addition to losing energy, a positron can directly annihilate with a free or bound electron before being thermalized. As the thermalization distance $(\Delta x)_{\text{th}}$ is predominantly covered while the positron is still relativistic, direct annihilation before thermalization also predominantly occurs during the relativistic regime (see below). We ignore the γ rays produced from such annihilation as the large positron velocity causes large shifts from the 0.511 MeV line emitted in the center-of-mass frame for the annihilating positron and electron. The quantity of interest to us is the probability for direct annihilation of the positron before

thermalization.

We first consider direct annihilation with free electrons. For a fast positron ($v \gg 2\pi\alpha c$) annihilating with a free electron at rest, the cross section is

$$\sigma_{\text{da,f}}^{\text{fast}} = \left(\frac{e^2}{m_e c^2} \right)^2 \frac{\pi}{\gamma + 1} \left[\frac{\gamma^2 + 4\gamma + 1}{\gamma^2 - 1} \ln(\gamma + \sqrt{\gamma^2 - 1}) - \frac{\gamma + 3}{\sqrt{\gamma^2 - 1}} \right]. \quad (51)$$

The above result ignores the Coulomb interaction between the positron and the electron. This interaction becomes important at lower positron velocities, for which the cross section [10] can be obtained by adding a ‘‘Coulomb focusing’’ factor to the low-velocity limit of the result in Eq. (51):

$$\sigma_{\text{da,f}}^{\text{slow}} = \left(\frac{e^2}{m_e c^2} \right)^2 \frac{2\pi^2 \alpha (c/v)^2}{1 - \exp(-2\pi\alpha c/v)}. \quad (52)$$

The probability for direct annihilation with free electrons before thermalization can be estimated as

$$P_{\text{da,f}} \sim Y_{e^-} \rho N_A \int_{\langle E_{e^+} \rangle}^{m_e c^2} \frac{\sigma_{\text{da,f}}^{\text{rel}} dE_{e^+}}{(dE_{e^+}/dx)_{\text{ex,pl}}} \sim \frac{1}{4B_{\text{rel}}} \int_1^{\langle \gamma \rangle} \frac{\ln(2\gamma)}{\gamma} d\gamma \sim 0.1, \quad (53)$$

where we have considered only the relativistic regime and used the excitation of free electrons as the dominant energy loss mechanism with $B_{\text{rel}} \sim 20$. Note that although for low positron velocities $\sigma_{\text{da,f}}^{\text{slow}}$ increases as $\sim 1/v^2$, this is cancelled by the same increase of the corresponding $-(dE_{e^+}/dx)_{\text{ex,pl}}$ [see Eq. (46)]. Thus, direct annihilation with free electrons before thermalization predominantly occurs when the predominant part of $(\Delta x)_{\text{th}}$ is covered, i.e., when the positron is still relativistic (see Sec. III A). Note also that the probability of this occurrence depends logarithmically on the initial positron energy and the density of the medium (through B_{rel}).

The cross section $\sigma_{\text{da,b}}^{\text{fast}}$ for direct annihilation of a fast positron with a bound electron in an atom (or ion) is the same as $\sigma_{\text{da,f}}^{\text{fast}}$. In contrast, for $v \lesssim \alpha c$,

$$\sigma_{\text{da,b}}^{\text{slow}} = \pi Z_{\text{eff}} \left(\frac{e^2}{m_e c^2} \right)^2 \frac{c}{v}, \quad (54)$$

where Z_{eff} is a function of v and depends on the atom (see Appendix D for the case of the H atom). The cross sections $\sigma_{\text{da,H}}^{\text{slow}}$ and $\sigma_{\text{da,He}}^{\text{slow}}$ for direct annihilation with the electrons in the H [11] and He [12] atoms, respectively, are compared with $\sigma_{\text{da,f}}^{\text{slow}}$ in Fig. 5. As $\sigma_{\text{da,f}}^{\text{slow}} > \sigma_{\text{da,H}}^{\text{slow}}$, $\sigma_{\text{da,He}}^{\text{slow}}$ and $Y_{e^-} \gg Y_{\text{H}}$, Y_{He} , the probability for direct annihilation with bound electrons at low positron velocities is much smaller than the corresponding probability in the case of

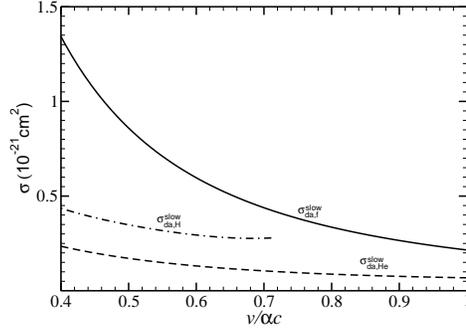


FIG. 5: Cross sections for direct annihilation of slow positrons with free electrons ($\sigma_{\text{da},f}^{\text{slow}}$, solid curve) and with the electrons in the H ($\sigma_{\text{da},\text{H}}^{\text{slow}}$ [11], dash-dotted curve) and He ($\sigma_{\text{da},\text{He}}^{\text{slow}}$ [12], dashed curve) atoms as functions of the positron velocity v in units of αc .

free electrons, which is already very small. On the other hand, inclusion of the bound electrons increases the number of targets for direct annihilation in the relativistic regime. This gives $P_{\text{da}} \approx P_{\text{da},f} + P_{\text{da},\text{H}} + P_{\text{da},\text{He}} \approx (Y_e/Y_{e^-})P_{\text{da},f}$, where P_{da} is the total probability of direct annihilation before thermalization and $Y_e/Y_{e^-} = 1.27$. Using the actual cross sections and rates of various energy loss processes over the entire thermalization regime, we have numerically calculated the probability of direct annihilation with free electrons before thermalization and found $P_{\text{da},f} = 9.52\%$. So the total probability including annihilation with bound electrons is $P_{\text{da}} \approx 12\%$.

C. Ps Formation before Thermalization

In addition to direct annihilation, positrons can form Ps with free and bound electrons before thermalization. As discussed above, direct annihilation predominantly occurs in the relativistic regime. As positrons become more and more nonrelativistic, Ps formation becomes more and more likely. The cross section for direct annihilation of slow positrons with free electrons multiplied by the number of free electrons per nucleon in the stellar surface region under consideration, $Y_{e^-}\sigma_{\text{da},f}^{\text{slow}}$, is compared in Fig. 6 with the corresponding quantities $Y_{e^-}\sigma_{\text{Ps},f}$, $Y_{\text{H}}\sigma_{\text{Ps},\text{H}}$, and $Y_{\text{He}}\sigma_{\text{Ps},\text{He}}$ for Ps formation with free electrons and the electrons in the H and He atoms, respectively. It can be seen that $Y_{\text{H}}\sigma_{\text{Ps},\text{H}}$ and $Y_{\text{He}}\sigma_{\text{Ps},\text{He}}$ are extremely large at $6.8 < E_{e^+}^{\text{kin}} < 100$ eV and $17.8 < E_{e^+}^{\text{kin}} < 250$ eV, respectively. As a result,

TABLE II: Probabilities and rates of various processes involved in the γ -ray emission from positron annihilation in the stellar surface region. The conditions in this region are characterized by $\rho = 1.59 \times 10^{-8} \text{ g cm}^{-3}$, $T = 1.53 \times 10^4 \text{ K}$, $Y_{e^-} \approx 0.67$, $Y_{\text{H}^+} \approx 0.667$, $Y_{\text{H}} \approx 0.033$, $Y_{\text{He}} \approx 7.33 \times 10^{-2}$, and $Y_{\text{He}^+} \approx 1.7 \times 10^{-3}$. Note that the rates for breakup and conversion of ${}^3\text{Ps}$ depend on the formation mode of ${}^3\text{Ps}$. The rates with the superscript “bt” correspond to the ${}^3\text{Ps}$ formed before thermalization and those with the superscript “Ps,H” correspond to the ${}^3\text{Ps}$ formed by the reaction $e^+ + \text{H} \rightarrow \text{Ps} + \text{H}^+$ after thermalization.

Processes	before thermalization	after thermalization
$e^+ + e^- \rightarrow \gamma + \gamma$	$P_{\text{da},f} = 9.52\%$	$\lambda_{\text{da},f} = 7.7 \times 10^2 \text{ s}^{-1}$
$e^+ + \text{H} \rightarrow \text{H}^+ + \gamma + \gamma$	$P_{\text{da},\text{H}} \approx 0.47\%$	$\lambda_{\text{da},\text{H}} \approx 13 \text{ s}^{-1}$
$e^+ + \text{He} \rightarrow \text{He}^+ + \gamma + \gamma$	$P_{\text{da},\text{He}} \approx 2.08\%$	$\lambda_{\text{da},\text{He}} \approx 15 \text{ s}^{-1}$
$e^+ + e^- \rightarrow \text{Ps} + \gamma$	$P_{\text{Ps},f} \ll 1\%$	$\lambda_{\text{Ps},f} = 4.6 \times 10^3 \text{ s}^{-1}$
$e^+ + \text{H} \rightarrow \text{Ps} + \text{H}^+$	$P_{\text{Ps},\text{H}} \approx 1\%$	$\lambda_{\text{Ps},\text{H}} \approx 9.9 \times 10^4 \text{ s}^{-1}$
$e^+ + \text{He} \rightarrow \text{Ps} + \text{He}^+$	$P_{\text{Ps},\text{He}} \approx 3\%$	$\lambda_{\text{Ps},\text{He}} \approx 4.6 \text{ s}^{-1}$
$e^- + {}^3\text{Ps} \rightarrow e^- + e^+ + e^-$	$\lambda_{3 \rightarrow 0,f}^{\text{bt}} \approx 4.5 \times 10^8 \text{ s}^{-1}$	$\lambda_{3 \rightarrow 0,f}^{\text{Ps,H}} \approx 1.2 \times 10^7 \text{ s}^{-1}$
$\text{H} + {}^3\text{Ps} \rightarrow \text{H} + e^+ + e^-$	$\lambda_{3 \rightarrow 0,\text{H}}^{\text{bt}} \approx 7.9 \times 10^6 \text{ s}^{-1}$	$\lambda_{3 \rightarrow 0,\text{H}}^{\text{Ps,H}} \approx 1.1 \times 10^5 \text{ s}^{-1}$
$\text{H}^+ + \text{Ps} \rightarrow \text{H} + e^+$	$\lambda_{3 \rightarrow 0,\text{H}^+}^{\text{bt}} \approx 7.7 \times 10^7 \text{ s}^{-1}$	$\lambda_{3 \rightarrow 0,\text{H}^+}^{\text{Ps,H}} \approx 3.2 \times 10^8 \text{ s}^{-1}$
$\text{He}^+ + \text{Ps} \rightarrow \text{He} + e^+$	$\lambda_{3 \rightarrow 0,\text{He}^+}^{\text{bt}} \approx 9.8 \times 10^4 \text{ s}^{-1}$	$\lambda_{3 \rightarrow 0,\text{He}^+}^{\text{Ps,He}} \approx 5.5 \times 10^4 \text{ s}^{-1}$
$e^- + {}^3\text{Ps} \rightarrow e^- + {}^1\text{Ps}$	$\lambda_{3 \rightarrow 1,f}^{\text{bt}} \approx 1.9 \times 10^6 \text{ s}^{-1}$	$\lambda_{3 \rightarrow 1,f}^{\text{Ps,H}} \approx 5.1 \times 10^8 \text{ s}^{-1}$
$\text{H} + {}^3\text{Ps} \rightarrow \text{H} + {}^1\text{Ps}$	$\lambda_{3 \rightarrow 1,\text{H}}^{\text{bt}} \approx 3.9 \times 10^6 \text{ s}^{-1}$	$\lambda_{3 \rightarrow 1,\text{H}}^{\text{Ps,H}} \approx 9.0 \times 10^6 \text{ s}^{-1}$

reactions are $e^- + {}^3\text{Ps} \rightarrow e^- + e^+ + e^-$ and $\text{H}^+ + \text{Ps} \rightarrow \text{H} + e^+$ with rates of $\approx 4.5 \times 10^8$ and $7.7 \times 10^7 \text{ s}^{-1}$, respectively [5]. The total rate for breakup of ${}^3\text{Ps}$ before thermalization is $\lambda_{3 \rightarrow 0}^{\text{bt}} \approx 5.3 \times 10^8 \text{ s}^{-1}$, to be compared with the rate of $\tau_{3\gamma}^{-1} = 7.04 \times 10^6 \text{ s}^{-1}$ for ${}^3\text{Ps}$ decay. The rates of the above breakup reactions and many other reactions involved in the γ -ray emission from positron annihilation are given in Table II for the adopted stellar conditions. Thus, before thermalization a fraction $(3/4)P_{\text{Ps}} \approx 3\%$ of the initial positrons form ${}^3\text{Ps}$, which are immediately broken up. The positrons released by the breakup reactions are quickly thermalized. As a result, effectively a fraction $1 - P_{\text{da}} - (P_{\text{Ps}}/4) \approx 87\%$ of the initial positrons are thermalized.

D. Fluxes of 0.511 MeV γ Rays

The thermal positrons again can directly annihilate with or form Ps with free or bound electrons. The rates for these processes are given in Table II for the adopted stellar conditions. The dominant reaction is Ps formation with the electron in the H atom with a rate of $\lambda_{\text{Ps,H}} = 9.9 \times 10^4 \text{ s}^{-1}$ [5]. The ^3Ps formed is quickly converted into ^1Ps or broken up. The dominant conversion reaction is $e^- + ^3\text{Ps} \rightarrow e^- + ^1\text{Ps}$ with a rate of $\lambda_{3 \rightarrow 1}^{\text{Ps,H}} = 5.1 \times 10^8 \text{ s}^{-1}$, and the dominant breakup reaction is $\text{H}^+ + \text{Ps} \rightarrow \text{H} + e^+$ with a rate of $\lambda_{3 \rightarrow 0}^{\text{Ps,H}} = 3.2 \times 10^8 \text{ s}^{-1}$ [5] (see also Table II). Whether directly formed or produced by the conversion reaction, all the ^1Ps immediately decay into two γ rays centered at 0.511 MeV with a FWHM of $\sim 2 \text{ keV}$ [5]. The positrons released by the breakup reaction are again quickly thermalized and follow the same fate of thermal positrons as outlined above.

Based on the discussion in the preceding subsections, a fraction $P_{\text{da}} \approx 12\%$ of the positrons produced by $\bar{\nu}_e$ absorption on protons directly annihilate and a fraction $P_{\text{Ps}} \approx 4\%$ form Ps before being thermalized, and the rest are thermalized on a timescale of $\sim 10^{-2} \text{ s}$, which is much shorter than the timescale of $\tau = 3 \text{ s}$ governing the production of the initial positrons. The positrons released by the breakup of ^3Ps are also quickly thermalized. As the positrons are produced approximately isotropically, their spatial distribution can be taken as uniform before and after thermalization. So in the region of interest to γ -ray emission, the time evolution for the numbers of various species per nucleon is governed by

$$\frac{dY_{1\text{Ps,bt}}}{dt} \approx \frac{1}{4}P_{\text{Ps}}\lambda_{\bar{\nu}_e p}(t) - \frac{Y_{1\text{Ps,bt}}}{\tau_{2\gamma}}, \quad (55)$$

$$\frac{dY_{3\text{Ps,bt}}}{dt} \approx \frac{3}{4}P_{\text{Ps}}\lambda_{\bar{\nu}_e p}(t) - \lambda_{3 \rightarrow 0}^{\text{bt}}Y_{3\text{Ps,bt}}, \quad (56)$$

$$\frac{dY_{e^+}}{dt} \approx (1 - P_{\text{da}} - P_{\text{Ps}})\lambda_{\bar{\nu}_e p}(t) + \lambda_{3 \rightarrow 0}^{\text{bt}}Y_{3\text{Ps,bt}} + \lambda_{3 \rightarrow 0}^{\text{Ps,H}}Y_{3\text{Ps}} - \lambda_{\text{Ps,H}}Y_{e^+}, \quad (57)$$

$$\frac{dY_{1\text{Ps}}}{dt} \approx \frac{1}{4}\lambda_{\text{Ps,H}}Y_{e^+} + \lambda_{3 \rightarrow 1}^{\text{Ps,H}}Y_{3\text{Ps}} - \frac{Y_{1\text{Ps}}}{\tau_{2\gamma}}, \quad (58)$$

$$\frac{dY_{3\text{Ps}}}{dt} \approx \frac{3}{4}\lambda_{\text{Ps,H}}Y_{e^+} - (\lambda_{3 \rightarrow 1}^{\text{Ps,H}} + \lambda_{3 \rightarrow 0}^{\text{Ps,H}})Y_{3\text{Ps}}, \quad (59)$$

where $Y_{1\text{Ps,bt}}$, $Y_{3\text{Ps,bt}}$, $Y_{1\text{Ps}}$, and $Y_{3\text{Ps}}$ correspond to the numbers per nucleon for the ^1Ps and ^3Ps formed before and after thermalization, and Y_{e^+} is the number of thermal positrons per nucleon. As the timescale of $\tau = 3 \text{ s}$ governing $\lambda_{\bar{\nu}_e p}(t)$ is much longer than $\tau_{2\gamma}$, $(\lambda_{3 \rightarrow 0}^{\text{bt}})^{-1}$, $(\lambda_{\text{Ps,H}})^{-1}$, and $(\lambda_{3 \rightarrow 1}^{\text{Ps,H}} + \lambda_{3 \rightarrow 0}^{\text{Ps,H}})^{-1}$, the above differential equations can be solved to good

approximation by setting all the time derivatives to zero. Thus, we have

$$Y_{1\text{Ps},\text{bt}}(t) \approx \frac{1}{4}P_{\text{Ps}}\lambda_{\bar{\nu}_ep}(t)\tau_{2\gamma}, \quad (60)$$

$$Y_{1\text{Ps}}(t) \approx \left(1 - P_{\text{da}} - \frac{1}{4}P_{\text{Ps}}\right)\lambda_{\bar{\nu}_ep}(t)\tau_{2\gamma}. \quad (61)$$

These results are equivalent to what is stated at the beginning of Sec. III and in Sec. III C: a fraction $P_{\text{Ps}}/4 \approx 1\%$ of the initial positrons form ^1Ps before thermalization and effectively a fraction $1 - P_{\text{da}} - (P_{\text{Ps}}/4) \approx 87\%$ of them form ^1Ps after thermalization.

Using a similar prescription to that for estimating the flux due to neutron capture on protons, we find that at radius $r > R$ the flux of 0.511 MeV γ rays from decay of the ^1Ps formed before thermalization is

$$\Phi_{\gamma(e^\pm),\text{bt}}(r, t_r) \approx \frac{Y_{1\text{Ps},\text{bt}}(t)}{4\tau_{2\gamma}} \left(\frac{R}{r}\right)^2 \rho N_A \int_0^d \exp\left(-\frac{d-x}{l_{\gamma(e^\pm)_e}}\right) dx, \quad (62)$$

$$\approx \frac{P_{\text{Ps}}\lambda_{\bar{\nu}_ep}(t)}{16} \left(\frac{R}{r}\right)^2 \rho N_A l_{\gamma(e^\pm)_e}, \quad (63)$$

$$\approx \frac{P_{\text{Ps}}E_B}{384\pi r^2 \langle E_{\bar{\nu}_e} \rangle \tau} \left(\frac{Y_p \langle \sigma_{\bar{\nu}_ep} \rangle}{Y_e \sigma_{\gamma(e^\pm)_e}}\right) \exp(-t/\tau), \quad (64)$$

$$\approx 7.8 \times 10^{-7} \left(\frac{1 \text{ kpc}}{r}\right)^2 \exp(-t/\tau) \text{ cm}^{-2} \text{ s}^{-1}, \quad (65)$$

where the factor $1/4$ in Eq. (62) comes from the integration of the local flux at a point in the stellar surface region over the forward solid angle. Note that although two 0.511 MeV γ rays are emitted in ^1Ps decay, only one contributes to the emergent flux (the other being emitted towards the stellar interior). Likewise, at radius $r > R$ the flux of 0.511 MeV γ rays from decay of the ^1Ps formed after thermalization is

$$\Phi_{\gamma(e^\pm)}(r, t_r) \approx \frac{[1 - P_{\text{da}} - (P_{\text{Ps}}/4)]E_B}{96\pi r^2 \langle E_{\bar{\nu}_e} \rangle \tau} \left(\frac{Y_p \langle \sigma_{\bar{\nu}_ep} \rangle}{Y_e \sigma_{\gamma(e^\pm)_e}}\right) \exp(-t/\tau), \quad (66)$$

$$\approx 6.8 \times 10^{-5} \left(\frac{1 \text{ kpc}}{r}\right)^2 \exp(-t/\tau) \text{ cm}^{-2} \text{ s}^{-1}. \quad (67)$$

The γ rays associated with $\Phi_{\gamma(e^\pm),\text{bt}}(r, t_r)$ and $\Phi_{\gamma(e^\pm)}(r, t_r)$ differ in that the former have a FWHM of ~ 6 keV while the latter have a FWHM of ~ 2 keV [5]. Note that $\Phi_{\gamma(e^\pm),\text{bt}}(r, t_r)$ has only a weak dependence on the density of the stellar surface region through P_{Ps} , which in turn depends logarithmically on the density through B_{nr} associated with the energy loss due to excitation of free electrons [see similar density dependence for $P_{\text{da},f}$ through B_{rel} as exhibited in Eq. (53)]. In contrast, apart from the weak density dependence of P_{da} and P_{Ps} ,

$\Phi_{\gamma(e^\pm)}(r, t_r)$ is sensitive to the breakup of ${}^3\text{Ps}$ and the conversion of ${}^3\text{Ps}$ into ${}^1\text{Ps}$, the rates of which are proportional to the density of the stellar surface region. For reasonable stellar conditions, $\Phi_{\gamma(e^\pm),\text{bt}}(r, t_r)$ is overwhelmed by $\Phi_{\gamma(e^\pm)}(r, t_r)$.

IV. DISCUSSION AND CONCLUSIONS

We have calculated the expected fluxes of 2.22 and 0.511 MeV γ rays from neutron capture on protons and positron annihilation, respectively, following $\bar{\nu}_e$ absorption on protons in the hydrogen envelope of an $11 M_\odot$ star that undergoes core collapse to produce a supernova. The γ -ray flux from neutron capture on protons exponentially decays on a timescale of $\tau_{\text{eff}} = 564$ s, which is determined by neutron decay and capture on protons and ${}^3\text{He}$ nuclei. The peak flux is $2.38 \times 10^{-7} \text{ cm}^{-2} \text{ s}^{-1}$ for a supernova at a distance of 1 kpc. In contrast, the γ -ray flux from positron annihilation follows the time evolution of the $\bar{\nu}_e$ luminosity. Although exponential decay on a timescale of $\tau = 3$ s is assumed here, the identical time evolution for the $\bar{\nu}_e$ luminosity and the γ -ray flux from positron annihilation holds in general so long as the timescales for thermalization of positrons and Ps formation are much shorter than ~ 1 s. The peak flux in this case is $6.8 \times 10^{-5} \text{ cm}^{-2} \text{ s}^{-1}$ for a supernova at a distance of 1 kpc. Detection of the γ -ray fluxes quoted above is beyond the capability of current instruments, and perhaps even those planned for the near future. For example, the proposed Advanced Compton Telescope [15] has a spectral resolution of 0.2–1% over the energy range of 0.2–10 MeV and an angular resolution of $\sim 1^\circ$, which are ideal for detecting the narrow γ -ray lines discussed here. This instrument has a projected sensitivity of $5 \times 10^{-7} \text{ cm}^{-2} \text{ s}^{-1}$ for narrow lines but an exposure time of 10^6 s is needed. As the fluxes of 2.22 and 0.511 MeV γ rays discussed here only last for $\sim 10^3$ and 10 s, respectively, their detection requires much more sensitive instruments.

If the γ -ray fluxes discussed here can be detected, they not only constitute a new kind of signals that occur during the gap of several hours between the neutrino signals and the optical display of a supernova, but may also provide a probe of the conditions in the surface layers of the supernova progenitor. For example, both the peak and the decay timescale τ_{eff} of the γ -ray flux from neutron capture on protons depend on the density of the stellar surface region. A higher density decreases the timescales for neutron capture on protons (τ_{np}) and ${}^3\text{He}$ nuclei (τ_{n3}), which increases the peak flux and decreases τ_{eff} . On the other

hand, a higher ${}^3\text{He}$ abundance decreases τ_{n3} , and hence τ_{eff} , but does not affect the peak flux as neutron capture on ${}^3\text{He}$ nuclei consumes neutrons without producing any γ ray. As another example, the rates for the breakup of ${}^3\text{Ps}$ and the conversion of ${}^3\text{Ps}$ into ${}^1\text{Ps}$ are proportional to the density of the stellar surface region. While the γ -ray flux from positron annihilation quoted above also applies approximately to higher densities than adopted here, for sufficiently smaller densities the ${}^3\text{Ps}$ formed would predominantly decay into three γ rays with a continuous spectrum instead of being broken up or converted. This would decrease the flux of 0.511 MeV γ rays from ${}^1\text{Ps}$ decay. In the limit where no ${}^3\text{Ps}$ are broken up or converted, this flux is reduced to 1/4 of the value estimated here. The above examples clearly illustrate that neutrino-induced γ -ray emission from the hydrogen envelope of a core-collapse supernova may serve as a useful probe of the conditions in the surface layers of the supernova progenitor.

Acknowledgments

We thank Wick Haxton for motivating us to carry out a detailed investigation of neutrino-induced γ -ray emission from supernovae, John Beacom for calling our attention to Ref. [2], and Icko Iben for providing the electronic file of the stellar model in Ref. [6]. We also thank Robert Gould and Richard Lingenfelter for helpful discussions. This work was supported in part by DOE grant DE-FG02-87ER40328.

APPENDIX A: CROSS SECTIONS FOR $\bar{\nu}_e$ ABSORPTION ON PROTONS AND COMPTON SCATTERING

In this appendix we set $\hbar = c = 1$. The cross section for the reaction $\bar{\nu}_e + p \rightarrow n + e^+$ is [16]

$$\begin{aligned} \sigma_{\bar{\nu}_e p} &= \frac{G_F^2 \cos^2 \theta_C}{\pi} (f^2 + 3g^2)(1 + \delta_R)(E_{\bar{\nu}_e} - \Delta)^2 \left\{ 1 - \frac{2[f^2 + 2(f + f_2)g + 5g^2]}{f^2 + 3g^2} \left(\frac{E_{\bar{\nu}_e}}{M_N} \right) \right\} \\ &= 9.56 \times 10^{-44} \left(\frac{E_{\bar{\nu}_e} - \Delta}{\text{MeV}} \right)^2 \left[1 - 7.2 \left(\frac{E_{\bar{\nu}_e}}{M_N} \right) \right] \text{ cm}^2, \end{aligned} \quad (\text{A1})$$

where G_F is the Fermi constant, θ_C is the Cabbibo angle with $\cos \theta_C = 0.9738$, $f = 1$ and $g = 1.27$ are the vector and axial vector coupling constants, $f_2 = 3.706$ is the anomalous nucleon isovector magnetic moment, $\delta_R \approx 0.024$ is the inner radiative corrections, $\Delta =$

$M_n - M_p = 1.293$ MeV is the difference between the neutron and proton masses M_n and M_p , and $M_N = (M_n + M_p)/2 = 938.9$ MeV.

The cross section for Compton scattering is

$$\sigma_{\gamma e} = \frac{\pi}{\epsilon_\gamma} \left(\frac{e^2}{m_e} \right)^2 \left[\left(1 - \frac{2}{\epsilon_\gamma} - \frac{2}{\epsilon_\gamma^2} \right) \ln(1 + 2\epsilon_\gamma) + \frac{1}{2} + \frac{4}{\epsilon_\gamma} - \frac{1}{2(1 + 2\epsilon_\gamma)^2} \right], \quad (\text{A2})$$

where e is the magnitude of the electron charge, m_e is the electron rest mass, and $\epsilon_\gamma = E_\gamma/m_e$ is the photon energy in units of m_e .

APPENDIX B: PARTITION FUNCTIONS OF ATOMS

The number of electron energy states in an isolated atom is infinite. This presents a problem in summing over these states to obtain the partition function of the atom as the sum formally diverges. However, the application of the partition function is sensible only when there are a large number of atoms. Consequently, the largest orbital radius of the electron in an atom is physically restricted to the interatomic distance. For our problem, the maximum radius r_{\max} can be estimated from

$$\frac{4\pi}{3} r_{\max}^3 \rho (Y_p + Y_\alpha) N_A = 1. \quad (\text{B1})$$

Take the H atom as an example. The largest orbital radius of the electron is related to the maximum principal quantum number n_{\max} as $r_{\max} \sim n_{\max}^2 \hbar^2 / (m_e e^2)$. For our adopted stellar conditions, $n_{\max} \sim 25$. The partition function of the H atom is then

$$g_{\text{H}} = 4 \sum_{n=1}^{n_{\max}} n^2 \exp \left[-\frac{I_{\text{H}}}{kT} \left(1 - \frac{1}{n^2} \right) \right] \approx 4.8, \quad (\text{B2})$$

where the factor of 4 comes from the spin states for the proton and the electron, and the factor n^2 accounts for the degeneracy of the orbital states of the n th energy level.

It can be seen that the partition function of the H atom under the stellar conditions of interest is dominated by the contribution from the ground state. This is also true for the He^+ ion and the He atom. As these two species are minor components in the stellar region of interest, we take their partition functions to be given approximately by the contributions from the corresponding ground states only, i.e., $g_{\text{He}^+} \approx 2$ and $g_{\text{He}} \approx 1$.

APPENDIX C: RATES OF POSITRON ENERGY LOSS

In addition to excitation of the free electrons in the plasma, positrons can also lose energy through excitation and ionization of the bound electrons in atoms and ions. Using the results from Ref. [17], we find that the energy loss rate per unit length of propagation for the latter process is

$$\begin{aligned} - \left(\frac{dE_{e^+}}{dx} \right)_{\text{ex,at}} &\approx 4\pi\rho N_A \left(\frac{e^4}{m_e v^2} \right) (Y_{\text{H}} B_{\text{H}} + 2Y_{\text{He}} B_{\text{He}}) \\ &= 4.88 \times 10^{-9} \left(\frac{c}{v} \right)^2 (Y_{\text{H}} B_{\text{H}} + 2Y_{\text{He}} B_{\text{He}}) \text{ MeV cm}^{-1}, \end{aligned} \quad (\text{C1})$$

where B_{H} and B_{He} are of the form

$$B = \ln \left[\frac{\gamma \sqrt{2\delta(\gamma-1)} m_e v c}{\overline{\Delta E}} \right] - \frac{1}{2} \left(\frac{v}{c} \right)^2 + b(\gamma, \delta). \quad (\text{C2})$$

In the above equation, $\overline{\Delta E}$ is the average excitation energy and $\overline{\Delta E} = 15$ and 41.5 eV for H and He atoms, respectively. In Eq. (C1) we have ignored the contributions from the He⁺ ions as their abundance is much smaller than the abundances of H and He atoms. Note that the energy loss due to excitation and ionization of the bound electrons in atoms and ions is significant only when the positron *kinetic* energy is $E_{e^+}^{\text{kin}} \gg \overline{\Delta E}$.

In the relativistic regime, three additional processes may be considered for positron energy loss. We follow the discussion in Ref. [18] and first consider bremsstrahlung. In general the energy loss rate in an ionized plasma differs from that in neutral matter. However, Ref. [18] showed that the rates are the same for these two cases for $\gamma \lesssim 10^2$. The relevant energy loss rate for our problem is

$$\begin{aligned} - \left(\frac{dE_{e^+}}{dx} \right)_{\text{brem}} &= 4\alpha \left(\frac{e^2}{m_e c^2} \right)^2 E_{e^+} (2Y_p + 6Y_\alpha) \left[\ln(2\gamma) - \frac{1}{3} \right] \\ &= 2.10 \times 10^{-11} \gamma \left[\ln(2\gamma) - \frac{1}{3} \right] \text{ MeV cm}^{-1}. \end{aligned} \quad (\text{C3})$$

Positrons can also lose energy through Compton scattering on the photons in the radiation field of the stellar surface region. The corresponding energy loss rate is

$$- \left(\frac{dE_{e^+}}{dx} \right)_{\text{Comp}} = \frac{32\pi}{9} \left(\frac{e^2}{m_e c^2} \right)^2 a_{\text{rad}} T^4 \gamma^2 = 2.30 \times 10^{-16} \gamma^2 \text{ MeV cm}^{-1}, \quad (\text{C4})$$

where a_{rad} is the radiation constant. In the presence of a magnetic field \mathcal{B} , positrons can lose energy through synchrotron radiation. This process is similar to Compton scattering

in that \mathcal{B} can be viewed as a source of virtual photons. The relative importance of these two processes can be gauged by comparing the energy densities in the magnetic and the radiation fields:

$$\frac{\mathcal{B}^2/(8\pi)}{a_{\text{rad}}T^4} = 0.959 \left(\frac{\mathcal{B}}{100 \text{ G}} \right)^2. \quad (\text{C5})$$

The energy loss rates $-(dE_{e^+}/dx)_{\text{ex,pl}}$, $-(dE_{e^+}/dx)_{\text{ex,at}}$, $-(dE_{e^+}/dx)_{\text{brem}}$, and $-(dE_{e^+}/dx)_{\text{Comp}}$ are compared in Fig. 4. Note that the last two rates increase with increasing γ (at least for the positron energies of interest here) whereas the first two rates decrease with increasing γ . Therefore, if the positron energy loss through bremsstrahlung and Compton scattering is unimportant in the relativistic regime, it can also be ignored in the nonrelativistic regime. Note also that $-(dE_{e^+}/dx)_{\text{ex,pl}}$ exceeds $-(dE_{e^+}/dx)_{\text{Comp}}$ by a factor of at least $\sim 2 \times 10^5$. So the positron energy loss through synchrotron radiation can be ignored for $\mathcal{B} \ll 4 \times 10^4 \text{ G}$. We assume that $\mathcal{B} \ll 4 \times 10^4 \text{ G}$ in the surface region of the star under consideration.

APPENDIX D: CROSS SECTIONS FOR DIRECT ANNIHILATION OF POSITRONS AND POSITRONIUM FORMATION

As an example of direct annihilation with bound electrons, we give the cross section $\sigma_{\text{da,H}}^{\text{slow}}$ for annihilation of a slow positron with the electron in the H atom [11]:

$$\sigma_{\text{da,H}}^{\text{slow}} = \pi Z_{\text{eff,H}} \left(\frac{e^2}{m_e c^2} \right)^2 \frac{c}{v}, \quad (\text{D1})$$

where $Z_{\text{eff,H}}$ is a function of the positron velocity v and can be approximated as

$$\begin{aligned} Z_{\text{eff,H}} \approx & 8.868 - 7.838 \left(\frac{v}{\alpha c} \right) - 102.77 \left(\frac{v}{\alpha c} \right)^2 + 527.38 \left(\frac{v}{\alpha c} \right)^3 \\ & - 978.68 \left(\frac{v}{\alpha c} \right)^4 + 773.15 \left(\frac{v}{\alpha c} \right)^5 - 197.17 \left(\frac{v}{\alpha c} \right)^6. \end{aligned} \quad (\text{D2})$$

The above approximation of $Z_{\text{eff,H}}$ is valid for $v \lesssim 0.7\alpha c$, which corresponds to positron kinetic energy of $E_{e^+}^{\text{kin}} < I_{\text{H}}/2 = 6.8 \text{ eV}$, i.e., below the threshold for Ps formation with the electron in the H atom. The cross sections $\sigma_{\text{da,f}}^{\text{slow}}$, $\sigma_{\text{da,H}}^{\text{slow}}$, and $\sigma_{\text{da,He}}^{\text{slow}}$ [12] are compared in Fig. 5.

The relative importance of direct annihilation and Ps formation depends on $E_{e^+}^{\text{kin}}$. Direct annihilation is dominant in the relativistic regime. As the positron becomes more and more

nonrelativistic, Ps formation becomes more and more important. The cross section for a nonrelativistic positron to form a Ps with a free electron at rest is (see e.g., [10, 19])

$$\sigma_{\text{Ps},f} = \frac{2^7 \pi \alpha}{3^{3/2}} \left(\frac{\hbar}{m_e c} \right)^2 \sum_{n=1}^{\infty} \frac{g_n/n}{u(u+1)}, \quad (\text{D3})$$

where $u = n^2 E_{e^+}^{\text{kin}}/I_{\text{H}}$ and g_n is the Gaunt factor for forming the Ps in the energy state with principal quantum number n . The Gaunt factor is close to unity and can be approximated as [20]

$$g_n \approx 1 + 0.1728 \left[\frac{u-1}{n^{2/3}(u+1)^{2/3}} \right] - 0.0496 \left[\frac{u^2 + (4/3)u + 1}{n^{4/3}(u+1)^{4/3}} \right]. \quad (\text{D4})$$

The calculation of the cross sections for Ps formation with bound electrons is rather complex. Here we use the measured cross sections $\sigma_{\text{Ps},\text{H}}$ and $\sigma_{\text{Ps},\text{He}}$ for Ps formation with the electrons in the H [13] and He [14] atoms, respectively. The cross section for direct annihilation with free electrons multiplied by the number of free electrons per nucleon in the stellar surface region under consideration, $Y_{e^-} \sigma_{\text{da},f}^{\text{low}}$, is compared in Fig. 6 with the corresponding quantities $Y_{e^-} \sigma_{\text{Ps},f}$, $Y_{\text{H}} \sigma_{\text{Ps},\text{H}}$, and $Y_{\text{He}} \sigma_{\text{Ps},\text{He}}$ for Ps formation with free electrons and the electrons in the H and He atoms, respectively.

-
- [1] G. S. Bisnovaty-Kogan, V. S. Imshennik, D. K. Nadyozhin, and V. M. Chechetkin, *Astrophys. Space Science* **35**, 23 (1975).
 - [2] O. G. Ryazhskaya, *Nuovo Cimento C* **22**, 115 (1999).
 - [3] X.-M. Hua and R. E. Lingenfelter, *Astrophys. J.* **319**, 555 (1987).
 - [4] Bussard, R. W., Ramaty, R., and Drachman, R. J., *Astrophys. J.* **228**, 928 (1979).
 - [5] R. J. Murphy, G. H. Share, J. G. Skibo, and B. Kozlovsky, *Astrophys. J. Suppl. Ser.* **161**, 495 (2005).
 - [6] C. Ritossa, E. Garcia-Berro, and I. Iben, Jr., *Astrophys. J.* **515**, 381 (1999); I. Iben, Jr., private communication (2005).
 - [7] E. Segrè, *Nuclei and Particles* (Benjamin/Cummings Publishing Company, Reading, Massachusetts), p. 624.
 - [8] E. Segrè, *Nuclei and Particles* (Benjamin/Cummings Publishing Company, Reading, Massachusetts), p. 450.
 - [9] R. J. Gould, *Physica* **60**, 145 (1972).

- [10] R. J. Gould, *Astrophys. J.* **344**, 232 (1989).
- [11] A. K. Bhatia, R. J. Drachman, and A. Temkin, *Phys. Rev. A* **16**, 1719 (1977).
- [12] J. W. Humberston, *J. Phys. B* **7**, L286 (1974).
- [13] S. Zhou, H. Li, W. E. Kauppila, C. K. Kwan, and T. S. Stein, *Phys. Rev. A* **55**, 361 (1997).
- [14] N. Overton, R. J. Mills, and P. G. Coleman, *J. Phys. B* **26**, 3951 (1993).
- [15] S. E. Boggs et al., preprint astro-ph/0608532.
- [16] P. Vogel and J. F. Beacom, *Phys. Rev. D* **60**, 053003 (1999).
- [17] R. J. Gould, *Physica* **62**, 555 (1972).
- [18] R. J. Gould, *Astrophys. J.* **196**, 689 (1975).
- [19] R. J. Gould, *Ann. Phys.* **69**, 321 (1972).
- [20] M. J. Seaton, *Monthly Notice of Royal Astronomical Society* **119**, 81 (1959).